Nanoscale Electrostatic Modulation of Mega-Ampere Electron Current in Solid-Density Plasmas

R. Li,[1,2] T. W. Huang,[1,*] L. B. Ju◉,[1] M. Y. Yu,[1] H. Zhang,[1] S. Z. Wu,[1] H. B. Zhuo,[1] C. T. Zhou,[1,†] and S. C. Ruan[1,‡]

[1]*Shenzhen Key Laboratory of Ultraintense Laser and Advanced Material Technology,*
Center for Advanced Material Diagnostic Technology, and College of Engineering Physics, Shenzhen Technology University,
Shenzhen 518118, People's Republic of China
[2]*College of Physics and Optoelectronic Engineering, Shenzhen University, Shenzhen 518060, People's Republic of China*

Transport of high-current relativistic electron beams in dense plasmas is of interest in many areas of research. However, so far the mechanism of such beam-plasma interaction is still not well understood due to the appearance of small time- and space-scale effects. Here we identify a new regime of electron beam transport in solid-density plasma, where kinetic effects that develop on small time and space scales play a dominant role. Our three-dimensional particle-in-cell simulations show that in this regime the electron beam can evolve into layered short microelectron bunches when collisions are relatively weak. The phenomenon is attributed to a secondary instability, on the space- and timescales of the electron skin depth (tens of nanometers) and few femtoseconds of strong electrostatic modulation of the microelectron current filaments formed by Weibel-like instability of the original electron beam. Analytical analysis on the amplitude, scale length, and excitation condition of the self-generated electrostatic fields is clearly validated by the simulations.

The transport of high-energy charged particle beams in plasma is relevant to many fields of physics, ranging from the microscopic plasma kinetics [1] to astrophysics [2]. The high-energy charged particle (e.g., electron) beam can encounter Coulomb collisions and collective effects [3]. The latter gives rise to plasma microinstabilities and leads to growing electric and/or magnetic fields, which in turn deflect or thermalize the beam and plasma. This process is attracting great interest in astrophysics as it is suspected to underlie the formation of collisionless shocks, the generation of giant magnetic fields, and the emission of afterglow radiation in the Universe [4–6]. Understanding such process also underpins many novel applications of high-power lasers in realizing high-energy density matters [7,8], high-gain inertial confinement fusion schemes [9–12], and compact particle and radiation sources [13–19].

There are many investigations of high-energy charged particle beam transport in plasma [20–30]. In particular, ultrashort ultraintense (USUI) laser pulses provide a favorable platform for generating high-energy electron beams. When interacting with a solid target, USUI laser pulses can accelerate the target-surface electrons to several MeV energies within a single light cycle [31], resulting in relativistic electron beams (REBs) with mega-ampere currents. Such high-current REB propagation in dense plasma can suffer from current filamentation instabilities (CFIs) [32,33] that break the beam into parallel narrow filaments with high-current density. During the process, strong magnetic fields are generated and amplified, which

in turn can cause the filaments to merge and form larger filaments [5,20,30]. On the timescale of ion motion, the self-generated magnetic fields can eventually destroy the ion filament [34].

Recently, attention has been given to the evolution of the CFIs [35–37] and, in experiments, large-scale (10–100 μm) current filaments and intense magnetic fields have been detected [29,30]. However, the evolution of the resulting current filaments, with their transverse dimension on the order of the skin depth $\delta = c/\omega_p$, where c is the vacuum light speed and ω_p is the background-plasma frequency, is still unclear. For solid-density plasmas, the skin depth $\delta \ll 0.1$ μm is not resolved in the experiments [25–30]. Moreover, typical fluid and/or hybrid simulations usually invoke Ohm's law to describe the electromagnetic fields induced by the REB, so that small spatiotemporal effects are also not included [38–41]. As a result, the dynamics and evolution of the microscopic filaments are still not well understood.

In this Letter, we report a new secondary filamentation scenario on the kinetic electron scale related to the microscopic electron current filaments and that such process significantly affects the beam evolution in dense plasma. Based on particle-in-cell simulations, we found two distinct evolution regimes for electron current filaments, corresponding to magnetic and electrostatic modulation, respectively, governed by the parameter $\eta = \nu_c/\omega_p$, where ν_c is the collision frequency between the background electrons and ions. For $\eta < 0.5$, strong oscillating electrostatic fields

are excited around the filaments and they become dominant in the REB evolution even when the ambient plasma is of solid density. As a result, instead of merging, the filaments further break up into nanoscale bunches along the REB propagation direction, a phenomenon not discussed previously. Theoretical analysis of the amplitude and distribution of the electromagnetic fields agrees well with the simulation results, revealing a robust regime for nanoscale beam modulation in dense plasmas.

We first conduct three-dimensional (3D) collisional particle-in-cell (PIC) simulations for REB propagation in solid-density plasma using the EPOCH code (version 4.17.8) [42]. For simplicity, the REB is cold and of uniform density $n_b = 6.3 \times 10^{21}$ cm^{-3} and current density $j_b = 3.0 \times 10^{13}$ A/cm^2, and the initial momentum is $p_{x0} \approx 5.7 m_e c$, where m_e is the electron rest mass. Its radius R_b is much larger than δ. The background-plasma density considered is $n_p = 1.2$ (case L) and 7.8×10^{23} cm^{-3} (case H), and its initial temperature is $T_e \sim 100$ eV. These parameters are common in laboratory intense laser- and beam-solid interactions [38]. Such REB can be readily generated by irradiating a solid-density target with a laser of intensity $10^{20} \sim 10^{21}$ W/cm^2. The collisions are two-body, with $\eta \propto Z\sqrt{n_p}$, where $Z = 2$, and 13 for the L and H cases is the charge number of the aluminum ion. Collisions of all plasma particles are taken into account, but those involving the rarefied beam electrons are neglected (see Sec. 2 of the Supplemental Material [43] for details). The simulation box is $L_x \times L_y \times L_z = 2.0 \times 1.0 \times 1.0$ μm. The spatial resolution is $\Delta x = \Delta y = \Delta z = 0.002$ μm, which well resolves the skin depth δ. The simulation box is filled with homogeneous plasma and the REB enters from the $x = 0$ boundary along the x direction, with five particles of each species in each grid. The simulation results are convergent under the present parameters.

Depending on η, two distinct regimes of the REB evolution are found, as shown in Fig. 1. Figure 1(a) for the high-density case H, where $\eta \sim 1$, shows that the REB breaks up transversely into narrow filaments. Figure 1(b) for the low-density case L, with $\eta \sim 0.1$, shows that the REB is broken up both transversely and longitudinally into microelectron bunches (MEBs). More details can be seen in the x, y-plane profiles of the beam density and corresponding magnetic field. Figure 1(c) shows that in the case H, the REB first breaks up into thin filaments and then they merge into larger ones, as to be expected of classical beam filamentation [29,30,35–37]. However, Fig. 1(d) for the case L shows that the REBs first break up into filaments, but then they become periodically modulated along the propagation direction and break up into short MEBs. The evolution of electric and magnetic energy components for both cases are shown in Fig. 1(e). When the REB arrives at the selected region ($0.7 < x < 0.8$ μm) around $t = 2.3$ fs, in both cases $|E_x|^2$ (red curves) undergoes a large jump, corresponding to the longitudinal electric field carried by the beam head, while $|E_y|^2$ and $|B_z|^2$ (green and blue curves) grow somewhat slower, as in filamentation instabilities due to space-charge effects [47]. In case H, $|E_x|^2$ then remains nearly constant for a short time before decreasing and saturating at a weaker level, together with $|E_y|^2$ and $|B_z|^2$. However, in case L, electric fields continue to grow exponentially (note the log scale) after the magnetic field is saturated around $t = 3.0$ fs, but at a distinctly slower rate, suggesting onset of a secondary electrostatic instability that should be responsible for the nanoscale modulation of narrow current filaments. It seems
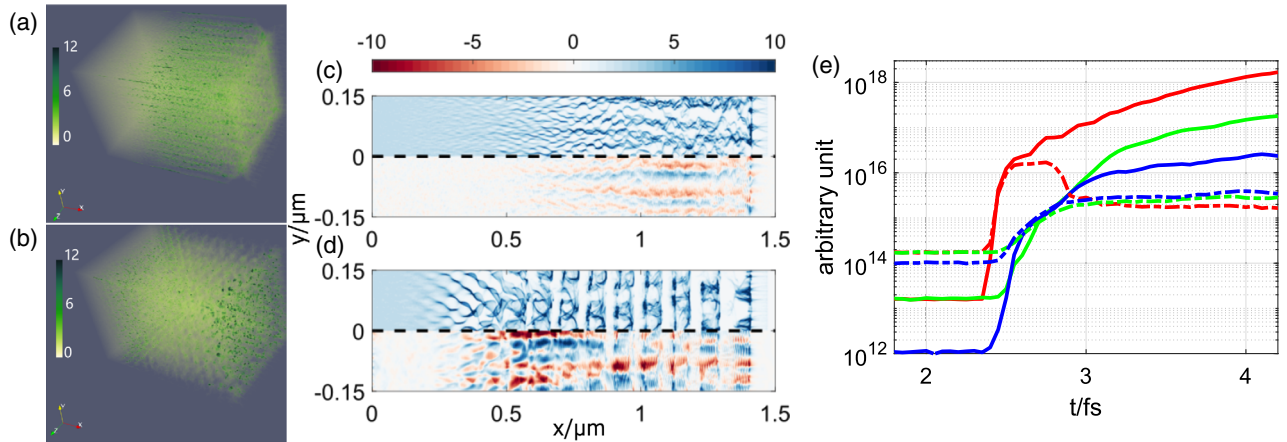

FIG. 1. Results at $t = 5$ fs from 3D PIC simulations. (a),(b) 3D distribution of n_b. (c),(d) n_b and B_z in the x, y plane at $z = 0$. In each panel, the top half is for n_b and the bottom half is for B_z. Here, (a) and (c) are for the H case, and (b) and (d) are for the L case. (e) Evolution of the electric and magnetic fields in the region ($0.7 < x < 0.8$ μm, $z = 0$), with the red curves for $|E_x|^2$, green curves for $|E_y|^2$, and blue curves for $|B_z|^2$. The solid and dashed curves are for the L and H cases, respectively. Unless otherwise stated (also in the following figures), the length, time, density, and electric and magnetic fields are in units of micrometers, 1 fs, n_b, 3×10^{11} V/m, and 10^3 T, respectively.

existing works have not considered such a secondary instability of the microfilaments. Under our parameters, the secondary instability is not due to the longitudinal two-stream instability, which is affected by collisions and grows at a much smaller rate [48].

To see the microscopic dynamics, we have carried out 2D simulations of a thin current filament on the skin-depth scale (say, $R_b \sim \delta$) for both H and L cases. Figure 2 is for the filament-electron density and the electric and magnetic fields. As expected, Figs. 2(d) and 2(h) show that in both cases the filament is surrounded by magnetic fields. But there is a clear difference in the electric field structures. Case L is associated with strong longitudinal as well as transverse periodic electric field perturbations, resulting in very different density structures in the two cases, as can be seen in Figs. 2(a) and 2(e). In particular, in case H the filament remains magnetically confined, but in case L the

filament breaks up into short MEBs, with the electrons between the bunches expelled from the axis region by the transverse electric fields. Such microscopic result is consistent with that from the preceding 3D simulation: after the REB filamentation, for case H the filaments are magnetically confined and can merge with each other to form larger ones, as shown in Figs. 1(a) and 1(c). For case L, the filaments are modulated by the strong transverse electric fields and break up into short bunches along the propagation direction, forming nanoscale MEBs, as shown in Figs. 1(b) and 1(d).

The results above can be understood in terms of a simple analytical model as follows. At first, the electric fields around the microelectron filament ($\tilde{x} - \beta_0 \tilde{t} < 0$, assuming that the position of filament head initially locates at $\tilde{x} = 0$) are (see Sec. 6 of the Supplemental Material [43] for details)

$$E_x \sim \frac{en_b u_0}{\varepsilon_0 \omega_p} \left[\eta - \exp\left(\frac{\eta(\tilde{x} - \beta_0 \tilde{t})}{2\beta_0}\right) \sin\left(\frac{\tilde{x} - \beta_0 \tilde{t}}{\beta_0}\right) \right] [1 - \exp(-\tilde{R}_b)\cosh(\tilde{y})],$$

$$E_y \sim -\frac{en_b u_0}{\varepsilon_0 \omega_p} \exp\left(\frac{\eta(\tilde{x} - \beta_0 \tilde{t})}{2\beta_0}\right) \cos\left(\frac{\tilde{x} - \beta_0 \tilde{t}}{\beta_0}\right) \exp(-\tilde{R}_b)\sinh(\tilde{y}), \tag{1}$$

where $(\tilde{x}, \tilde{y}, \tilde{R}_b) = (x, y, R_b)\omega_p/c$, $\tilde{t} = t\omega_p$, and $\beta_0 = u_0/c$ is the normalized initial beam velocity. We can see that there are oscillating electric fields in both longitudinal and transverse directions, and an Ohmic electric field (the η term in the first square brackets of E_x) in the longitudinal

direction. The oscillating fields result from the response of the background electrons to the REB and depend strongly on η. They are electrostatic since $\partial_x E_y - \partial_y E_x = 0$ for $\eta \to 0$. In case H for strong collisions, the oscillating electric field is damped, so that only the Ohmic and
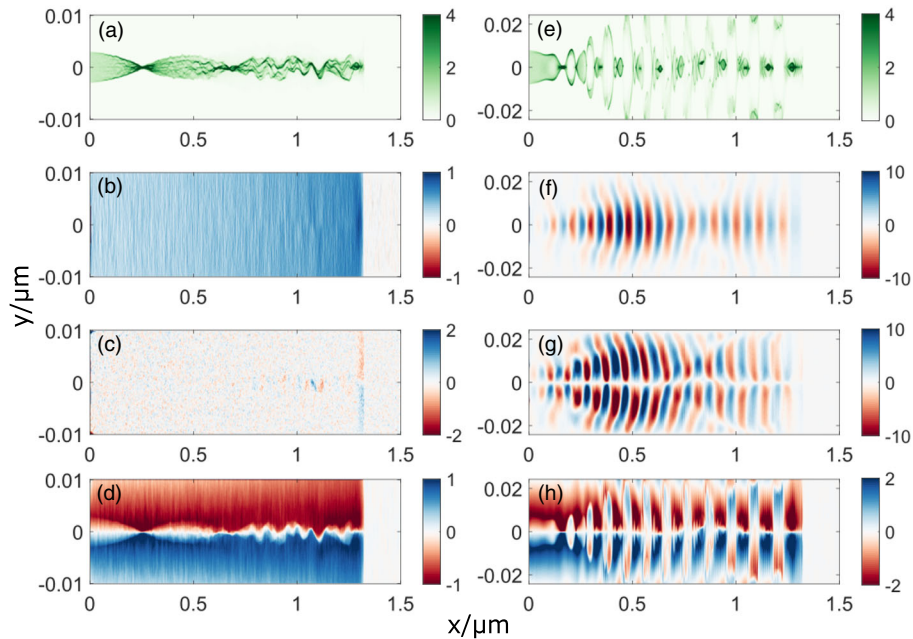

FIG. 2. Evolution of a single microelectron filament in dense plasma from 2D PIC simulations. The left and right panels are for the cases H and L, respectively. (a) and (e) Filament-electron densities. (b) and (f) E_x. (c) and (g) E_y. (d) and (h) B_z.
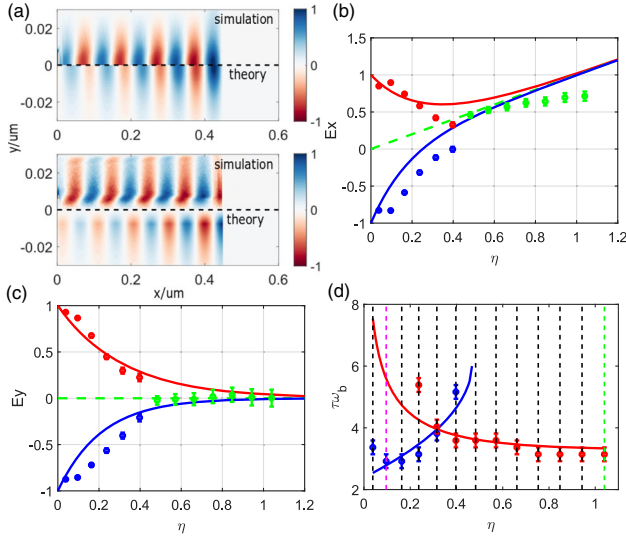
FIG. 3. (a) Electric field structures of the microelectron filament from the simulation and theory for case L at an early stage. The upper panel is for E_x and the bottom panel is for E_y. (b),(c) E_x and E_y versus η. The solid curves are from the model and the dots with error bars are from the simulations. The red and blue curves in (b) are for E_x at the positions $[(\tilde{x} - \beta_0\tilde{t})/\beta_0] = -\frac{5}{2}\pi$ and $-\frac{7}{2}\pi$, respectively. The red and blue curves in (c) are for E_y at $[(\tilde{x} - \beta_0\tilde{t})/\beta_0] = -3\pi$ and -2π, respectively. The dashed green lines mark the limit $\eta \to 1$. (d) Normalized characteristic times of electrostatic modulation ($\tau_{\mathrm{mod}}\omega_b$) and magnetic pinching ($\tau_{\mathrm{pin}}\omega_b$) in the laboratory frame versus η. The blue and red curves are from Eqs. (3) and (4), respectively.

magnetic fields remain. In case L for weak collisions, however, oscillating electric fields survive and become the dominant fields.

Figure 3(a) shows that the amplitude and spatial distribution of the electric fields obtained from the theory agree well with the simulation results. With increase of η (or collisions), E_x changes from the oscillating one to the typical Ohmic field, and the transverse oscillating electric field E_y is gradually damped, which is clearly validated by the simulations, as shown in Figs. 3(b) and 3(c). In addition, for $\eta < 0.5$, both longitudinal and transverse oscillating electric fields can be easily identified (see the red and blue dots), and their amplitudes decrease as the value of η increases. For $\eta > 0.5$, the Ohmic field dominates and the transverse electric field becomes negligible, as shown by the green dots. Note that for $\eta \sim 1$ the Ohmic field from the simulation is less than that from the theory. This can be attributed to background-electron heating, which is self-consistently included in the simulation but not in the theory. Plasma heating can reduce the value of η and thus the Ohmic field since $\eta \propto T_e^{-3/2}$.

The nanoscale modulation of the microfilament can be visualized by looking into the dynamics of filament electrons. In the beam rest frame x' (the quantities in this frame are primed, if needed), with the filament located in

$-\infty < x' < 0$ and the background plasma moves with velocity $\mathbf{v}_0 = -u_0\hat{\mathbf{x}}$, the motion of the beam electrons can approximately be described by

$$\frac{d^2\tilde{y}}{d\tilde{t}'^2} + \tilde{\omega}'^2(\tilde{x}')\tilde{y} = 0, \qquad (2)$$

where $\tilde{\omega}'(\tilde{x}') = (\sqrt{\gamma_0}\omega_b/\omega_p) \exp[-(\tilde{R}_b/2)] \times \sqrt{\beta_0^2 - \exp(\eta\tilde{x}'/2\gamma_0\beta_0)\cos(\tilde{r}')}$, $\tilde{r}' = (\tilde{x}'/\gamma_0\beta_0) + (3\eta/2)$, $\omega_b = \sqrt{e^2 n_b/\epsilon_0 m_e}$ is the beam plasma frequency, $(\tilde{x}', \tilde{y}, \tilde{R}_b) = (x', y, R_b)\omega_p'/c$, $\tilde{t}' = t'\omega_p'$, and $\gamma_0 = 1/\sqrt{1-\beta_0^2}$. The approximation $\sinh(\tilde{y}) \sim \tilde{y}$ has been used, since here $|\tilde{y}| \leq 1$. The above equation shows that the electrons execute harmonic transverse motion given by $\tilde{y}(\tilde{t}') = \tilde{R}_b\cos(\tilde{\omega}'\tilde{t}')$, where the frequency $\tilde{\omega}'(\tilde{x}')$ can be regarded as the bounce frequency [49–51] and depends on the longitudinal position for $\eta \ll 1$. This is caused by the initial nonuniformity of oscillating E_y' along the longitudinal direction. The neighboring beam electrons oscillate at different frequencies along the x direction, with those at larger frequencies moving toward the beam axis faster than those at lower frequencies, causing the nonuniformity of the filament density n_b' along the x direction. As a result, the unevenness of E_y' along the longitudinal direction becomes enhanced since $E_y' \propto n_b'$ and the phase of E_y' is synchronous with that of $\tilde{\omega}'$, thereby resulting in the secondary instability and breaking of the electron filament into short bunches. We note that the longitudinal nonuniformity of the bounce frequency originates from the transverse electrostatic field rather than magnetic field and exists in both the beam and plasma rest frames [52].

In view of the transverse dynamics of beam filaments, one can assume that when the difference between the maximum and minimum transverse size of the electron filament reaches half its initial radius, the electrostatic modulation becomes important. Then the characteristic time of electrostatic modulation ($\tilde{\tau}_{\mathrm{mod}}'$) can be defined by

$$\cos(\omega_{\min}'\tilde{\tau}_{\mathrm{mod}}') - \cos(\omega_{\max}'\tilde{\tau}_{\mathrm{mod}}') = \frac{1}{2}, \qquad (3)$$

where $\omega_{\min}' \approx (\sqrt{\gamma_0}\omega_b/\omega_p)\exp[-(\tilde{R}_b/2)]\sqrt{\beta_0^2 - \exp(-\pi\eta)}$ and $\omega_{\max}' \approx (\sqrt{\gamma_0}\omega_b/\omega_p)\exp[-(\tilde{R}_b/2)]\sqrt{\beta_0^2 + \exp[-\pi(\eta/2)]}$. Correspondingly, the characteristic time of magnetic modulation or pinching ($\tilde{\tau}_{\mathrm{pin}}'$) can be described by the reduction of the maximum transverse size of the electron filament to half of its initial radius, which leads to

$$\tilde{\tau}_{\mathrm{pin}}' = \frac{1}{\omega_{\min}'}\arccos\left(\frac{1}{2}\right). \qquad (4)$$

Figure 3(d) shows that, with increase of η, τ_{pin} decreases but τ_{mod} increases, and they reach the same value at around $\eta \sim 0.3$, agreeing well with the simulation results.

This indicates the transition from electrostatic modulation to magnetic modulation with increase of η. If $\eta \geq 0.5$, Eq. (3) has no solution, suggesting that the filament cannot be modulated by the electrostatic fields, which become too weak as analyzed above.

In experiments, the condition for nanoscale electrostatic modulation ($\eta < 0.5$) is common for dense plasma with low ion charge number or high temperature, since $\eta \propto (Z/T_e^{3/2})$. For example, it can be important for REB propagation in DT plasma for controlled fusion, even when the density is compressed to, say 10^{24} cm^{-3} (see Sec. 4 in the Supplemental Material [43] for the simulation results). If the temperature is so high that the solid is fully ionized, η can be much smaller than unity. For example, graphite can be fully ionized at $T_e \sim 500$ eV, leading to $\eta \sim 0.1$. A fully ionized aluminum target at $T_e \sim 1$ keV also results in $\eta \sim 0.1$. In both cases, electrostatic modulation is dominant, as shown by our simulations in Sec. 5 of the Supplemental Material [43], where details of the experimental parameters, including the beam density, beam temperature, and divergency angle, and ionization effect are also discussed.

In summary, our collisional PIC simulations and analytical model reveal the existence of a new regime of high-current electron beam transport in solid-density plasma, where the REB can break up into nanoscale electron bunches by self-excited strong oscillating transverse electrostatic fields if collisions are relatively weak. In this regime of kinetic beam-plasma interaction, the ultrafast nanoscale modulation dominates the beam transport and can potentially lead to novel applications. For example, the strong electric fields in solid-density plasmas can be a source of heating in high-energy density situations. In addition, the nanoscale electron bunch wiggling in the strong plasma fields can emit incoherent x- or gamma-ray photons with a duration comparable with the electron bunch. Thus, attosecond x or γ rays may also be generated.

---

[*] taiwu.huang@sztu.edu.cn

[†] zcangtao@sztu.edu.cn

[‡] scruan@sztu.edu.cn

[1] C. Ruyer *et al.*, Nat. Phys. **16**, 983 (2020).

[2] B. A. Remington, R. P. Drake, and D. D. Ryutov, Rev. Mod. Phys. **78**, 755 (2006).

[3] F. F. Chen, *Introduction to Plasma Physics and Controlled Fusion* (Plenum Press, New York, 1984).

[4] S. V. Lebedev, A. Frank, and D. D. Ryutov, Rev. Mod. Phys. **91**, 025002 (2019).

[5] M. V. Medvedev, M. Fiore, R. A. Fonseca, L. O. Silva, and W. B. Mori, Astrophys. J. **618**, L75 (2005).

[6] A. Achterberg and J. Wiersma, Astron. Astrophys. **475**, 1 (2007); A. Achterberg, J. Wiersma, and C. A. Norman, Astron. Astrophys. **475**, 19 (2007).

[7] K. Matsuo, N. Higashi, N. Iwata, S. Sakata, S. Lee *et al.*, Phys. Rev. Lett. **124**, 035001 (2020).

[8] H. Sawada, Y. Sentoku, T. Yabuuchi, U. Zastrau, E. Förster, F. N. Beg, H. Chen, A. J. Kemp, H. S. McLean, P. K. Patel, and Y. Ping, Phys. Rev. Lett. **122**, 155002 (2019).

[9] M. Tabak, J. Hammer, M. E. Glinsky, W. L. Kruer, S. C. Wilks, J. Woodworth, E. M. Campbell, M. D. Perry, and R. J. Mason, Phys. Plasmas **1**, 1626 (1994).

[10] H. B. Zhuo, Z. L. Chen, Z. M. Sheng, M. Chen, T. Yabuuchi, M. Tampo, M. Y. Yu, X. H. Yang, C. T. Zhou, K. A. Tanaka, J. Zhang, and R. Kodama, Phys. Rev. Lett. **112**, 215003 (2014).

[11] L. C. Jarrott *et al.*, Nat. Phys. **12**, 499 (2016).

[12] F. Zhang *et al.*, Nat. Phys. **16**, 810 (2020).

[13] H. Sawada, C. M. Salinas, F. N. Beg, H. Chen, A. J. Link, H. S. McLean, P. K. Patel, Y. Ping, and G. J. Williams, Plasma Phys. Controlled Fusion **62**, 065001 (2020).

[14] K. W. D. Ledingham, I. Spencer, T. McCanny, R. P. Singhal, M. I. K. Santala *et al.*, Phys. Rev. Lett. **84**, 899 (2000).

[15] N. P. Dover, M. Nishiuchi, H. Sakaki, Ko. Kondo, M. A. Alkhimova *et al.*, Phys. Rev. Lett. **124**, 084802 (2020).

[16] G. Q. Liao, Y-T. Li, Y.-H. Zhang, H. Liu, X.-L. Ge *et al.*, Phys. Rev. Lett. **116**, 205003 (2016).

[17] A. Benedetti, M. Tamburini, and C. H. Keitel, Nat. Photonics **12**, 319 (2018).

[18] G. J. Williams *et al.*, Phys. Plasmas **23**, 123109 (2016).

[19] D. P. Higginson *et al.*, Phys. Plasmas **26**, 012113 (2019).

[20] B. Allen, V. Yakimenko, M. Babzien, M. Fedurin, K. Kusche, and P. Muggli, Phys. Rev. Lett. **109**, 185007 (2012).

[21] Y. Fang, V. E. Yakimenko, M. Babzien, M. Fedurin, K. P. Kusche, R. Malone, J. Vieira, W. B. Mori, and P. Muggli, Phys. Rev. Lett. **112**, 045001 (2014).

[22] M. Shaikh, A. D. Lad, G. Birindelli, K. Pepitone, J. Jha, D. Sarkar, S. Tata, G. Chatterjee, I. Dey, K. Jana, P. K. Singh, V. T. Tikhonchuk, P. P. Rajeev, and G. Ravindra Kumar, Phys. Rev. Lett. **120**, 065001 (2018).

[23] Y. Sentoku, E. d'Humières, L. Romagnani, P. Audebert, and J. Fuchs, Phys. Rev. Lett. **107**, 135005 (2011).

[24] R. Jung, J. Osterholz, K. Löwenbröck, S. Kiselev, G. Pretzler, A. Pukhov, O. Willi, S. Kar, M. Borghesi, W. Nazarov, S. Karsch, R. Clarke, and D. Neely, Phys. Rev. Lett. **94**, 195001 (2005).

[25] J. Fuchs, T. E. Cowan, P. Audebert, H. Ruhl, L. Gremillet *et al.*, Phys. Rev. Lett. **91**, 255002 (2003).

[26] M. Manclossi, J. J. Santos, D. Batani, J. Faure, A. Debayle, V. T. Tikhonchuk, and V. Malka, Phys. Rev. Lett. **96**, 125002 (2006).

[27] K. L. Lancaster, J. S. Green, D. S. Hey, K. U. Akli, J. R. Davies *et al.*, Phys. Rev. Lett. **98**, 125002 (2007).

[28] G. F. Swadling, C. Bruulsema, F. Fiuza, D. P. Higginson, C. M. Huntington, H-S. Park, B. B. Pollock, W. Rozmus, H. G. Rinderknecht, J. Katz, A. Birkel, and J. S. Ross, Phys. Rev. Lett. **124**, 215001 (2020).

[29] G. Chatterjee *et al.*, Sci. Rep. **7**, 8347 (2017).

[30] L. Romagnani, A. P. L. Robinson, R. J. Clarke, D. Doria, L. Lancia, W. Nazarov, M. M. Notley, A. Pipahl, K. Quinn, B. Ramakrishna, P. A. Wilson, J. Fuchs, O. Willi, and M. Borghesi, Phys. Rev. Lett. **122,** 025001 (2019).

[31] P. Gibbon, *Short Pulse Laser Interaction with Matter* (Imperial College Press, London, 2005).

[32] B. Hao, Z. M. Sheng, C. Ren, and J. Zhang, Phys. Rev. E **79,** 046409 (2009).

[33] A. Bret, L. Gremillet, D. Bénisti, and E. Lefebvre, Phys. Rev. Lett. **100,** 205008 (2008).

[34] C. Ruyer and F. Fiuza, Phys. Rev. Lett. **120,** 245002 (2018).

[35] A. Grassi, M. Grech, F. Amiranoff, F. Pegoraro, A. Macchi, and C. Riconda, Phys. Rev. E **95,** 023203 (2017).

[36] O. Polomarov, I. Kaganovich, and G. Shvets, Phys. Rev. Lett. **101,** 175001 (2008).

[37] T. N. Kato, Phys. Plasmas **12,** 080705 (2005).

[38] A. P. L. Robinson, D. J. Strozzi, J. R. Davies, L. Gremillet, J. J. Honrubia, T. Johzaki, R. J. Kingham, M. Sherlock, and A. A. Solodov, Nucl. Fusion **54,** 054003 (2014).

[39] H. Xu, X. H. Yang, J. Liu, and M. Borghesi, Plasma Phys. Controlled Fusion **61,** 025010 (2019).

[40] C. T. Zhou, X. T. He, and M. Y. Yu, Phys. Plasmas **13,** 092109 (2006).

[41] C. T. Zhou, X. T. He, and M. Y. Yu, Appl. Phys. Lett. **92,** 071502 (2008).

[42] T. D. Arber *et al.*, Plasma Phys. Controlled Fusion **57,** 113001 (2015).

[43] See Supplemental Material at http://link.aps.org/supplemental/10.1103/PhysRevLett.127.245002 for the discussions on particle collisions, the influence of two-stream instability, the simulation of REB transport in DT plasma, the discussions on experimental conditions, and the derivation of electromagnetic fields and analysis of filament modulation mechanism, which includes Refs. [32,39–41,44–46].

[44] D. A. Hammer and N. Rostoker, Phys. Fluids **13,** 1831 (1970).

[45] L. A. Conttrill, A. B. Langdon, B. F. Lasinski, S. M. Lund, K. Molvig, M. Tabak, R. P. J. Town, and A. Williams, Phys. Plasmas **15,** 082108 (2008).

[46] R. A. B. Alraddadi, A. P. L. Robinson, J. Pasley, and N. C. Woolsey, Phys. Plasmas **25,** 023104 (2018).

[47] M. Tzoufras, C. Ren, F. S. Tsung, J. W. Tonge, W. B. Mori, M. Fiore, R. A. Fonseca, and L. O. Silva, Phys. Rev. Lett. **96,** 105002 (2006).

[48] For our parameters, the longitudinal two-stream instability is suppressed by collisions and can only grow up on a much later time in case L [43] (Sec. 3).

[49] R. F. Lutomirski and R. N. Sudan, Phys. Rev. **147,** 156 (1966).

[50] R. C. Davidson, D. A. Hammer, I. Haber, and C. E. Wagner, Phys. Fluids **15,** 317 (1972).

[51] A. Bret, A. Stockem, F. Fiuza, C. Ruyer, L. Gremillet, R. Narayan, and L. O. Silva, Phys. Plasmas **20,** 042102 (2013).

[52] The transverse motion of filament electrons and the resulting response of background plasma will generate transverse net current j_y. However, the increase of j_y could not generate a significant longitudinal gradient in B_z according to $-(\partial B_z/\partial x) = \mu_0 j_y + \mu_0\varepsilon_0(\partial E_y/\partial t) \simeq 0$. This is because j_y is actually the electrostatic response of E_y and is canceled with the displacement current $\varepsilon_0\partial_t E_y$. Thus, B_z does not contribute to the nonuniformity of the bounce frequency since $\partial_x B_z \simeq 0$ during the linear stage [43] (Sec. 6).